Title

Mapping sulcal pattern asymmetry and local cortical surface gray matter distribution in vivo: maturation in perisylvian cortices.

Journal

Cerebral cortex (New York, N.Y. : 1991), 12(1)

ISSN

1047-3211

Authors

Sowell, Elizabeth R
Thompson, Paul M
Rex, David
et al.

Publication Date

2002

DOI

10.1093/cercor/12.1.17

Peer reviewed

Mapping Sulcal Pattern Asymmetry and Local Cortical Surface Gray Matter Distribution *In Vivo*: Maturation in Perisylvian Cortices

Elizabeth R. Sowell, Paul M. Thompson, David Rex, David Kornsand, Kevin D. Tessner, Terry L. Jernigan[1] and Arthur W. Toga

Department of Neurology, Laboratory of Neuro Imaging, University of California, Los Angeles, Los Angeles, CA and [1]Department of Veterans Affairs Medical Center and Departments of Psychiatry and Radiology, University of California, San Diego, School of Medicine, San Diego, CA, USA

Previous *in vivo* morphometric studies of human brain maturation between childhood and young adulthood have revealed a spatial and temporal pattern of progressive brain changes that is consistent with the *post mortem* cytoarchitectonic and cognitive developmental literatures. In this study, we mapped age differences in structural asymmetries at the cortical surface in groups of normally developing children (7–11 years), adolescents (12–16 years) and young adults (23–30 years) using novel surface-based mesh modeling image analytic methods. We also assessed relationships between cortical surface sulcal asymmetry and the local density of the underlying cortical gray matter. Results from this study reveal that perisylvian sulcal asymmetries are much more prominent in the adults than in the children studied. The superior posterior extent of the Sylvian fissure in the right hemisphere is ~7 mm more superior in the average adult than in the average child studied, whereas little difference is observed during this age range in the location of this anatomical structure in the left hemisphere. Age-related differences in Sylvian fissure asymmetry were significant ($P = 0.0129$, permutation test), showing increased asymmetry with increasing age. We also show age-related increases in local gray matter proportion bilaterally in the temporo-parietal cortices that are anatomically and temporally related to the sulcal asymmetries. Results from this cross-sectional study imply that asymmetries in the Sylvian fissure are dynamically changing into young adulthood and show that variability in brain tissue density is related to asymmetry in this region. These morphological differences may be related to changing cognitive abilities and are relevant in interpreting results from studies of abnormal brain development where perisylvian brain regions are implicated.

Introduction

To date, most neurodevelopmental structural magnetic resonance imaging (MRI) studies have focused on abnormally developing populations of infants, children and adolescents, and numerous morphometric abnormalities have been reported. Age-matched comparison groups are typically used as the standard to interpret results from individuals with various neurodevelopmental and neuropsychiatric abnormalities, and inferences are made at these static points in development. Ideally, brain dysmorphology should be interpreted differently for different age groups, but relatively few studies of normative brain maturation have been conducted to allow interpretation of the findings from abnormal populations from a broader developmental perspective.

Normative MRI studies of human brain maturation conducted thus far have revealed dynamic, regionally variable morphologic changes occurring between childhood and young adulthood (Jernigan *et al.*, 1991; Pfefferbaum *et al.*, 1994; Caviness *et al.*, 1996; Giedd *et al.*, 1996a,b, 1999; Reiss *et al.*, 1996; Sowell and Jernigan, 1998). Findings such as gray matter volume reductions in dorsal frontal and parietal regions between childhood and young adulthood have been reported (Jernigan *et al.*, 1991; Sowell and Jernigan, 1998). Recently, newer methods have been employed to assess brain maturational changes on a voxel-by-voxel basis (Paus *et al.*, 1999; Sowell *et al.*, 1999a,b). These studies have shown a spatial and temporal pattern of progressive changes consistent with earlier volumetric studies and consistent with regional patterns of cellular maturational events such as myelination (Yakovlev and Lecours, 1967; Benes *et al.*, 1994) and changing synaptic density (Huttenlocher, 1979; Huttenlocher and de Courten, 1987). Specifically, dorsal parietal and frontal cortices mature between childhood and adolescence (Sowell *et al.*, 1999a). After adolescence, a striking new pattern is observed where parietal changes nearly cease and a dramatic increase in frontal and striatal maturation occurs (Sowell *et al.*, 1999b). In another recent study, we reported accelerated brain growth in frontal and lateral temporal brain regions during the post-adolescent years (Sowell *et al.*, 2001). Notably, we found an inverse relationship between gray matter density reduction and late brain growth that appeared to be specific to dorsal frontal regions, and we also found some evidence for a gray matter density increase localized to the perisylvian cortex bilaterally.

In *post mortem* studies, sulcal and gyral landmarks on the surface of the brain have been used to demarcate anatomical regions that are functionally significant and correlated with cytoarchitectonically derived tissue maps of human brain structure (Brodmann, 1909). Asymmetries in these sulcal patterns have also been of considerable interest, particularly in perisylvian cortices given the functional lateralization of language in this region (Geschwind and Galaburda, 1985). *Post mortem* studies have shown that in adults, the Sylvian fissure is longer (extends further posterior) in the left hemisphere than the right (Galaburda *et al.*, 1978; Ide *et al.*, 1996), and *in vivo* vascular imaging studies have shown that the Sylvian fissure angles up more dramatically at its posterior end in the right hemisphere than the left (LeMay and Culebras, 1972). Recent *in vivo* MRI studies of brain surface morphology have shown similar effects in normal individuals studied as controls for clinical populations (Thompson *et al.*, 1998; Narr *et al.*, 2001) where the Sylvian fissure posterior limit is ~10 mm further back in the left than the right hemisphere and the slope is greater in the right hemisphere than the left when all subjects' brain data are fixed in a standardized coordinate system. Left greater than right hemisphere perisylvian asymmetries (planum temporale length) have also been observed in *post mortem* studies of infants, suggesting a preprogrammed biological substrate for functional asymmetries (Witelson and Pallie, 1973).

Little is yet known about the emergence of cortical surface gyral and sulcal asymmetries in normal development. While *in vivo* volumetric and voxel-based morphometric analyses of human brain maturation have shown us spatially and temporally variable patterns of changing tissue compositions in different regions of the cerebral cortex, nothing is yet known about how these changes may relate to sulcal and gyral asymmetries at the

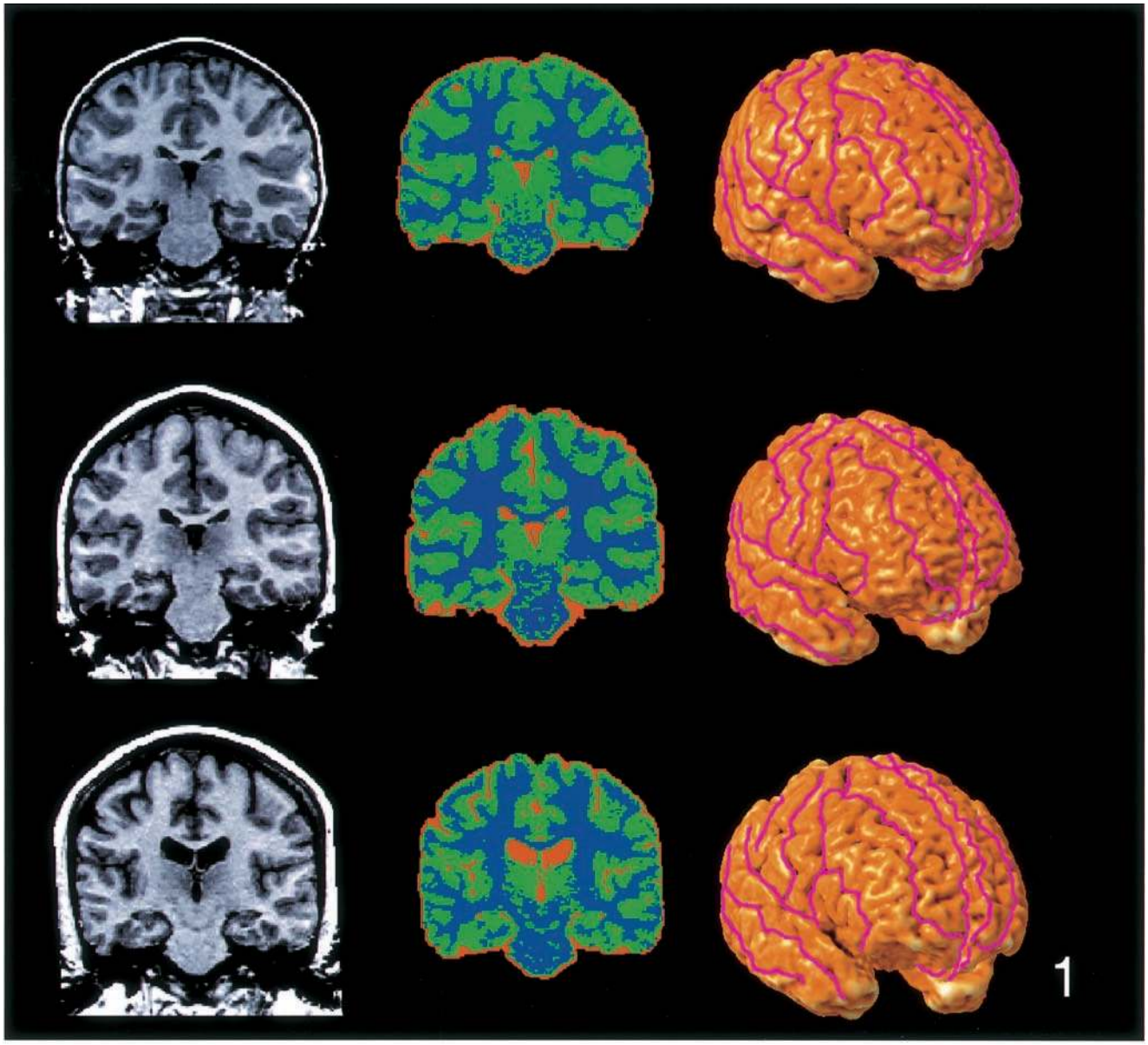
1

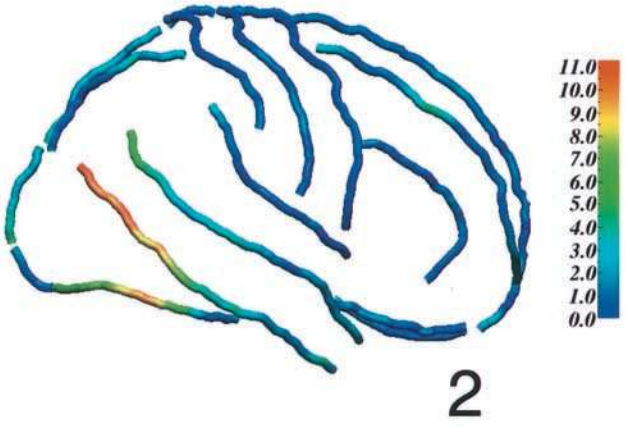
11.0
10.0
9.0
8.0
7.0
6.0
5.0
4.0
3.0
2.0
1.0
0.0
2

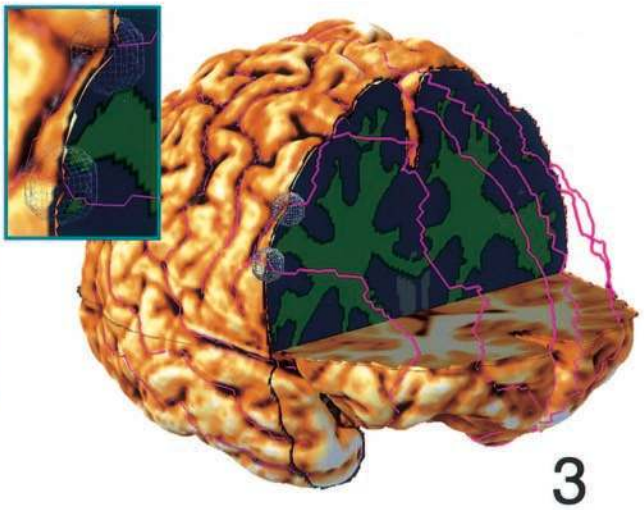
3

cortical surface. In the present study, we addressed these issues predicting that we would see age effects in sulcal asymmetry patterns that were regionally similar to the age effects observed in voxel-based morphometric analyses of gray matter tissue maps in the same subjects (Sowell *et al*., 1999a,b).

Materials and Methods

Subjects

Thirty-five subjects including 14 children (7–11 years; mean age 9.4 years; seven boys, seven girls), 11 adolescents (12–16 years; mean age 13.9 years; six boys, five girls) and 10 young adults (23–30 years; mean age 25.6 years; five men, five women) were studied with MRI. All child and adolescent subjects were recruited as normal controls for a large, multidisciplinary neurodevelopmental research center. Age ranges for the child and adolescent groups were chosen because they roughly correspond to pre-pubertal and pubertal status, though no direct measures of hormonal states were collected. These children were deemed medically and psychiatrically normal after extensive parent interviews, physical examinations and neuropsychological testing. Children with any history of learning disability or developmental delay were excluded. All of the children were right handed. Informed consent was obtained from all children and their parents. The 10 young adult subjects were recruited as normal controls for neuropsychiatric studies of adult patient populations. These subjects were thoroughly screened for medical, neurological and psychiatric disorders, and informed consent was obtained from each one.

Imaging Protocol

MR was performed with a 1.5 T magnet (Signa, General Electric, Milwaukee, WI). A gradient-echo (SPGR) T_1-weighted series was collected in the sagittal plane for each subject with T_R = 24 ms, T_E = 5 ms, N_{EX} = 2, flip angle = 45, field of view = 24 cm, 124 slices with section thickness of 1.2 mm, no gaps (shown in Fig. 1), with an imaging time of 19 min.

Image Pre-processing

The image pre-processing methods are described in detail in another report (Sowell *et al*., 1999a) and will be only briefly summarized here. Image data sets were subjected to the following preprocessing analyses: rigid-body reslicing of the volume into a standard orientation; interactive isolation of supratentorial cranial regions from surrounding extracranial and infratentorial tissue; three-dimensional (3D) digital filtering to reduce inhomogeneity artefacts (Sled *et al*., 1998); tissue segmentation using semi-automated algorithms (Kollokian, 1996); scaling into the ICBM-305 standard space (Mazziotta *et al*., 1995) using an automated 12-parameter linear transformation (Woods *et al*., 1993); and, finally, cortical surfaces were automatically extracted from each MR volume using a 3D active surface algorithm (MacDonald *et al*., 1994).

Reorientation

First, reslicing into a standard orientation was accomplished by trained operators 'tagging' 10 standardized anatomical landmarks in each subject's image data set that corresponded to the same 10 anatomical landmarks defined on the ICBM-305 average brain (Evans *et al*., 1994; Mazziotta *et al*., 1995). This reslicing step was performed only to provide image analysts with a standard view of the brain, making it easier to apply standardized rules for defining cerebral and non-cerebral regions.

Table 1
Summary of anatomical criteria for delineating sulci

Sulcus	Origin	Termination
Sylvian fissure	Anterior: lateral junction of temporal and frontal lobes	Posterior: superior posterior extent of ascending ramus
Superior temporal	Anterior: temporal pole on lateral surface	Posterior: superior posterior extent of ascending segment of parallel sulcus/angular gyrus
Inferior temporal	Anterior: temporal pole on lateral surface	Posterior: transverse occipital sulcus/temporo-occipital incisure
Central, pre/postcentral	Superior: interhemispheric fissure	Inferior: Sylvian fissure
Superior frontal	Anterior: mesial extent of frontal marginal sulcus	Posterior: precentral gyrus/sulcus
Inferior frontal	Anterior: inferior extent of lateral orbital sulcus	Posterior: precentral gyrus/sulcus
Intraparietal	Anterior: postcentral sulcus	Posterior: transverse occipital sulcus

Note: detailed anatomical criteria for defining these and other sulci can be found on the World Wide Web at http://www.loni.ucla.edu/~esowell/sulcvar.html.

Tissue Segmentation

Semi-automated tissue segmentation was then conducted for each volume data set to classify voxels based on signal value as most representative of gray matter, white matter, or cerebrospinal fluid (CSF). Sample tissue segmented images that correspond to the original grayscale images are shown in Figure 1.

Brain Masking

Tissue classified images were then used to aid in creating a mask of the brain where the CSF around the outer edge of the cortex (in most places) could be used as a predefined border between brain and scalp.

Spatial Filter

The brain masks were used to apply a 3D spatial filter to remove low-frequency changes, or 'drifts' in MR signal value across the volume and the images were resubmitted to the minimum distance classifier resulting in skull stripped, rf-corrected, tissue segmented volumes for each subject.

Spatial Normalization

Cerebellar and brain stem structures were manually defined and subtracted from each segmented volume. The supratentorial cranial volume (gray scale images) from each subject was scaled into standard ICBM-305 space using a completely automated 12 parameter linear transformation (Woods *et al*., 1993).

Figure 1. Sample original T_1-weighted (left), skull stripped tissue segmented (middle) images and surface rendering (right) with Sylvian fissure, superior and inferior temporal sulci, central, pre- and postcentral sulci, superior and inferior frontal sulci, and olfactory sulci all drawn in pink. The midline landmark curves bordering the interhemispheric fissure, which are necessary as limiters for the cortical surface matching algorithms, are also shown in pink. One representative subject from the child group is shown in the top row, from the adolescent group in the middle row and from the adult group in the bottom row.

Figure 2. Inter-rater reliability map representing the average difference (in millimeters of displacement) of six subjects' sulcal lines drawn by two raters. The magnitude of displacement is shown in color, coded according to the color bar on the right. Note that the average difference is <2 mm in most places. Reliability was worse in inferior posterior temporal and ventral occipital cortices (8–10 mm average difference between raters), the same regions where root mean square variability was highest in all three age groups.

Figure 3. Surface rendering of one representative subject with cut-out showing tissue segmented coronal slice and axial slice superimposed within the surface. Sulcal lines are shown where they would lie on the surface in the cut-out region. Note the sample spheres over the right hemisphere inferior frontal sulcus (lower sphere) and on the middle region of the precentral sulcus (upper sphere) that illustrate varying degrees of gray matter density. In the blown-up panel, note the upper sphere has a higher gray matter density than the lower sphere as it contains only blue pixels (gray matter) within the brain. The lower sphere also contains green pixels (white matter) that would lower the gray matter proportion within it. In the actual analysis, the gray matter proportion was measured within 15 mm spheres centered across every point over the cortical surface.

Cortical Surface Extraction

The automated surface extraction software (MacDonald *et al.*, 1994) creates a spherical mesh surface that is continuously deformed to fit a cortical surface tissue threshold intensity value (signal value which best differentiates cortical CSF on the outer surface of the brain from the underlying cortical gray matter) from the brain volume aligned in standard ICBM-305 space. The resulting cortical surfaces consist of 100 000–150 000 polygons that form a high-resolution mesh of discrete triangular elements (Thompson *et al.*, 1997; Thompson and Toga, 1997). Sample cortical surface renderings can be seen in Figure 1. Because of poor cortical surface extraction on the inferior surface of the brain relative to the dorsal and lateral surfaces in our young subjects, we have excluded results from these regions in our interpretation of the data.

Anatomical and Statistical Analyses

Cortical Surface Sulcal Line Drawings

Image analysts (D.K. and E.R.S.), who were blind to subject gender and age, drew each of 11 sulci (sylvian fissure and central, pre-central, post-central, superior temporal, inferior temporal, superior frontal, inferior frontal, intraparietal, olfactory and collateral sulci) in each hemisphere on the surface rendering of each subject's brain. In addition to contouring the major sulci, a set of seven midline landmark curves bordering the longitudinal fissure were outlined in each hemisphere to establish hemispheric gyral limits. Spatially registered gray-scale image volumes in coronal, axial and sagittal planes were available simultaneously to help disambiguate brain anatomy. A sample fully contoured surface rendering can be seen in Figure 1. We have developed detailed criteria, summarized briefly in Table 1, for delineating the cortical lines and for starting and stopping points for each sulcus. These criteria have previously been described briefly (Thompson *et al.*, 1997; Thompson and Toga, 1997; Narr *et al.*, 2001) and complete details of the written anatomical protocol can be found on the World Wide Web (at http://www.loni.ucla.edu/~esowell/sulcvar.html). It is important to note that, despite inter-individual variability in the continuity of external cortical sulci, all contours were drawn continuously over minor interruptions when they occurred (Ono *et al.*, 1990). While this procedure may somewhat oversimplify sulcal variability, it was necessary for group averaging of these sulci and to produce parametric models used to drive cortical surface matching algorithms (Thompson *et al.*, 1997, 2000b; Thompson and Toga, 1998).

Sulcal Line Averaging

Each sulcal contour was redigitized to contain x, y and z coordinates for 100 equidistant points. The mean of each point (within the child, adolescent and young adult groups) in each sulcal line was computed across subjects. Information regarding sulcal variability within each population was retained using these methods (Thompson and Toga, 1996, 1997, 1998; Thompson *et al.*, 1997). Asymmetry maps were derived from the sulcal averages, such that the distances in millimeters between analogous points on sulcal curves in one brain hemisphere and a reflected version (mirror image) of the opposite hemisphere were measured and mapped onto average cortical surface curves for each group. For all sulcal line asymmetry measures, the distances between analogous points in the two hemispheres were assessed only in the anterior–posterior and superior–inferior axes (y–z direction shift) and information regarding left–right (x direction) shift was not taken into account. This is because asymmetries in the left–right direction were not likely to capture the kinds of asymmetries reported in the temporal lobe sulci (superior–inferior or anterior–posterior) and were thought to more likely reflect increased sulcal depth, which was thought less relevant in the temporal lobe asymmetry analyses.

To assess the reliability of the anatomical methods, cortical surface lines were drawn independently by two raters (D.K. and E.R.S.) for six subjects' image volume data (right hemisphere only) using standardized rules from a written protocol. Inter-rater reliability was assessed in terms of millimeters difference between the two raters at each of 100 equidistant points along the average of each of the cortical surface lines. A 3D map of average disparity (in millimeters) between the average of the sulcal lines drawn for six subjects by rater 1 and the same lines drawn in the same six subjects by rater 2 is shown in Figure 2. Note that, in most regions, the average difference between raters was <2 mm, with the exception of posterior inferior temporal sulci and the colateral sulcus where the differences were up to 10 mm. Thus, group differences observed in posterior–inferior temporal cortices and on the inferior surface of the brain where reliability was relatively low are interpreted cautiously.

Cortical Surface and Local Gray Matter Proportion Averaging

Variability of cortical surfaces surrounding and between the sulcal contours was obtained using the averaged sulcal contours as anchors to drive 3D cortical surface mesh models from each subject into correspondence; the detailed methods have been described previously (Thompson *et al.*, 2000b, 2001). Intersubject differences in cortical surface anatomy were computed by measuring the amount of x, y, z coordinate shift in millimeters (or deformation) at each of 65 536 points along the cortical surface to match the cortical anatomy of one subject with another. Given that the deformation maps (acquired during cortical surface matching) associate the same cortical anatomy in each subject, a local measurement of gray matter proportion (at each point over the surface of the brain) could be made in each subject and averaged within groups. Briefly, a sphere with a radius of 15 mm centered at each cortical surface point was made and referenced to the same spatial location in the gray matter maps for each subject derived earlier in the tissue classification. The proportion of segmented gray matter pixels relative to the total number of pixels in this sphere was computed (at each point)

Figure 4. (*A*) Asymmetry maps for the child, adolescent and adult groups were created by subtracting the sulcal mesh averages of one hemisphere from the mirror of the other hemisphere to create vectors representing displacement asymmetry (in millimeters) in the superior–inferior and anterior–posterior directions shown in color. These maps not only illustrate the average sulcal asymmetry in color, but also show differences in sulcal shape profiles between the hemispheres, since the right hemisphere is mapped onto the mirror of the left hemisphere and vice versa. Thus, the color coding is identical in the two hemispheres, but the shape of the right hemisphere sulci can be seen as distinct from the left hemisphere sulci. Note the left and right Sylvian fissures are close together (~11 mm displacement) in the children and more splayed (~16 mm displacement) in the young adults. (*B*) Ratio map of the asymmetry at each point on each sulcus (i.e. the distance in millimeters between analogous points on sulcal curves in one brain hemisphere and a mirror image of the opposite hemisphere) in the average child to the asymmetry at each point on each sulcus in the average adult. Increases and decreases are represented in color, where red regions are indicative of increases in asymmetry with age and pink regions are representative of decreases in asymmetry with age (according to the color bar on the right). Note the prominent increase in asymmetry over the length of the Sylvian fissure. Only one hemisphere is represented as it is a composite ratio measure of the right and left hemispheres combined (*C*) Probability map of the difference in asymmetry between the child group and the adult group represented as *P*-values (for age group effect on asymmetry between children and young adults) at each point along each sulcal curve according to the color bar on the right. The age group effect on asymmetry is significant for the Sylvian fissure ($P = 0.041$) as determined with permutation tests.

Figure 5. (*A*) Cortical surface variability maps in 3D viewed from the right and the left showing variability in the average child ($n = 14$), the average adolescent ($n = 11$) and the average young adult ($n = 10$). The color bar indicates patterns of variability within each group as the root mean square magnitude (in millimeters) of displacement vectors required to map each individual onto the group average surface mesh. Note that this map is representative of residual brain shape variability after affine transformation into ICBM-305 standard space. Higher variability is observed in the postcentral gyrus and posterior temporal regions in all three age groups, with relatively less variability in precentral and anterior temporal gyri. (*B*) Cortical gray matter proportion/density maps for the average child, adolescent and young adult groups. Gray matter density (the average proportion of voxels within a 15 mm sphere centered at the cortical surface that are tissue segmented as gray matter) is represented in color according to the color bar on the right. Warmer colors are representative of higher gray matter proportions (i.e. upper sphere in Fig. 3) and cooler colors of lower gray matter proportions (i.e. lower sphere in Fig. 3).

and stored as a map of gray matter proportion (with values 0.0–1.0), for each subject (see Fig. 3). The average local gray matter proportion was then computed for each analogous cortical point in each group. Note that the proportion of gray matter in each sphere is reflective, to some extent, of local cortical thickness that varies over different regions of the brain as a function of cytoarchitecture (Von Economo, 1929) and over time with maturation, likely from changes in myelination (Yakovlev and Lecours, 1967; Benes *et al.*, 1994) and synaptic density (Huttenlocher, 1979; Huttenlocher and de Courten, 1987). Maps of average gray matter proportion increase were created by comparing the average maps from each group at corresponding surface points. Note that we are focusing on the gray matter density increase shown in the perisylvian region in our previous report (Sowell *et al.*, 2001), given that we were interested in studying changes in asymmetry in the same region. These methods are similar to the well-established voxel-based morphometric methods used in earlier studies (Wright *et al.*, 1995; Sowell *et al.*, 1999a,b).

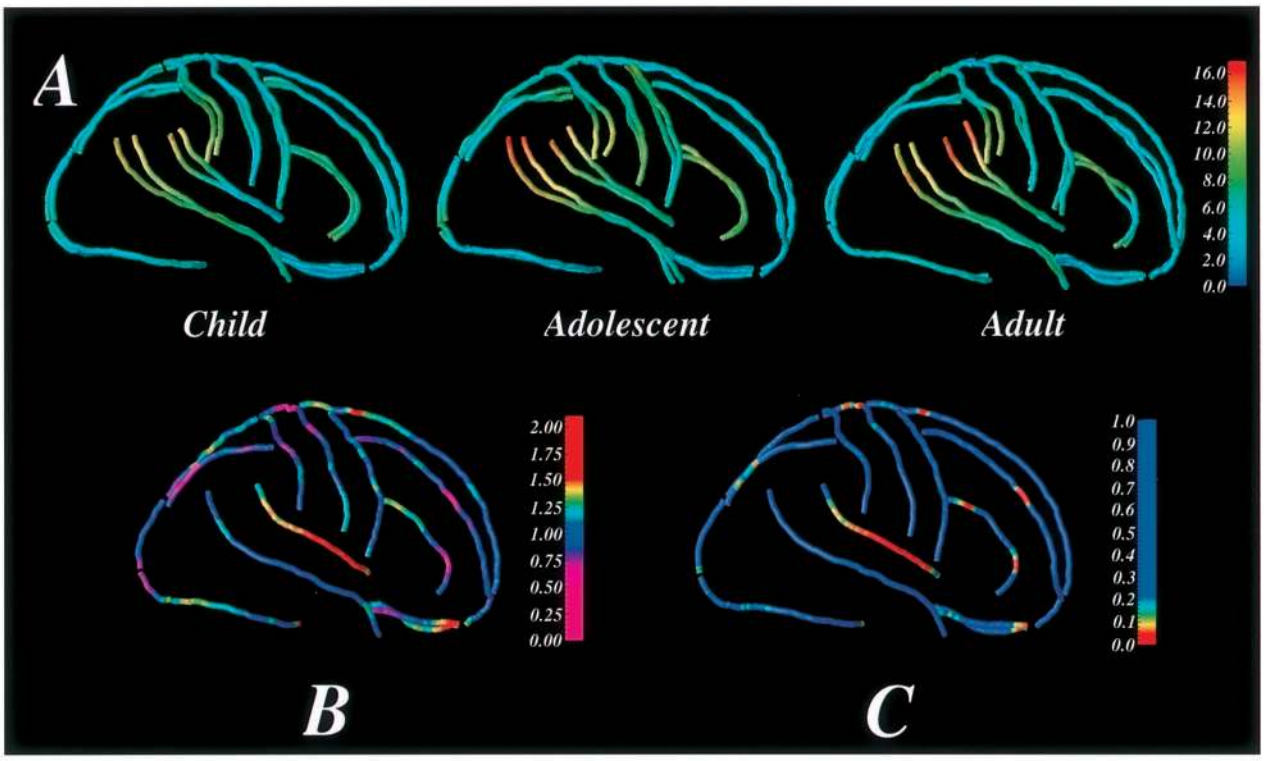

4

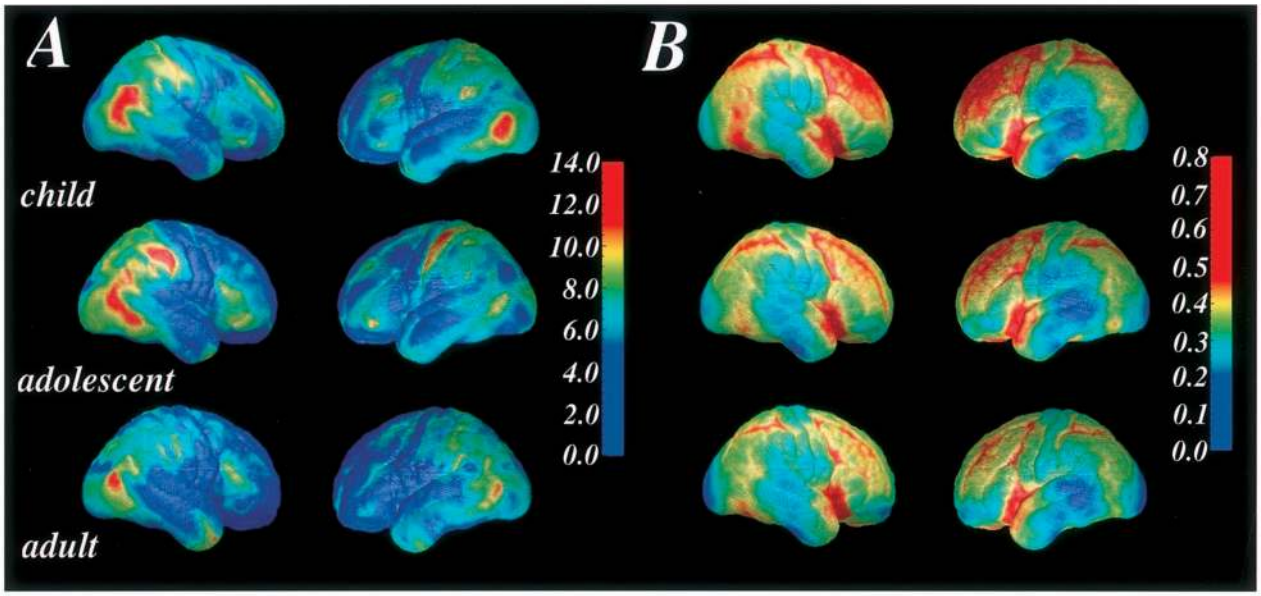

5

Table 2
Temporal lobe sulcal pattern summary by age-group and hemisphere

	Child			Adolescent			Adult		
	LH	RH	AS	LH	RH	AS	LH	RH	AS
Sylvian fissure									
Superior extreme	39 (8.7)	41 (7.7)	–0.037 (0.1)	36 (7.7)	43 (8.9)	–0.082 (0.1)	40 (7.0)	48 (6.8)	–0.090 (0.1)
Posterior extreme	–43 (7.6)	–38 (7.0)	0.062 (0.1)	–48 (5.2)	–39 (6.6)	0.101 (0.1)	–45 (7.9)	–35 (6.2)	0.125 (0.1)
Slope (si/ap)	0.79 (0.2)	0.90 (0.2)	–0.066 (0.2)	0.68 (0.1)	0.96 (0.3)	–0.160 (0.2)	0.79 (0.2)	1.10 (0.2)	–0.170 (0.1)
Superior temporal sulcus									
Superior extreme	36 (3.9)	38 (5.4)	–0.018 (0.1)	38 (7.1)	38 (8.5)	0.004 (0.1)	37 (7.3)	37 (5.3)	–0.011 (0.1)
	–70 (5.3)	–60 (10.6)	0.074 (.1)	–69 (4.7)	–61 (8.4)	0.060 (0.1)	–69 (5.2)	–62 (7.0)	0.055 (.1)
	0.80 (0.1)	0.94 (0.2)	–0.075 (0.1)	0.86 (0.2)	0.90 (0.2)	–0.019 (0.1)	0.83 (0.1)	0.90 (0.2)	–0.041 (0.1)

All extremes are reported as mean stereotaxic positions in millimeters, standard deviations are in parentheses; LH = left hemisphere, RH = right hemisphere, AS = (left-right)/(left + right) asymmetry, ap = anterior posterior extent, si = superior inferior extent.

Statistical Analyses

After the basic preprocessing steps were conducted for each individual, statistical maps of differences between the child and adult groups were created for sulcal asymmetry measures. Note that similar tests were conducted for the child to adolescent, and adolescent to adult groups, but only the child to adult contrasts are presented because change over the shorter age spans was not as robust. In these analyses, the correlation (Pearson's *r*) between group membership (i.e. child versus adult) and sulcal asymmetry (i.e. the distance in millimeters between analogous points on sulcal curves in one brain hemisphere and a mirror image of the opposite hemisphere) at each point on each sulcal line was calculated. For the asymmetry group difference statistical maps, a sulcal line point threshold of $P = 0.05$ was used and permutation tests were conducted to assess the overall significance of the statistical maps of group asymmetry difference in each sulcal line (at a threshold of $P = 0.05$) and to correct for multiple comparisons. In these analyses, subjects were randomly assigned to groups (i.e. child or adult group) for 10 000 new correlational analyses for each sulcal line (at each point on each sulcal line) and the number of significant results (i.e. asymmetry at any point on each sulcal line that significantly differed between groups at the threshold of $P = 0.05$) that occurred in the real group difference test was compared with the null distribution of significant results that occurred by chance in the permutation analyses for each sulcal line. To assess relationships between gray matter density and asymmetry, we conducted correlational analyses between the asymmetry measure and gray matter density at each point on the Sylvian fissure for the child, adolescent and young adult groups. We focused on the temporal lobe sulci for these analyses because that was where we expected to observe asymmetries and where we showed increases in gray matter density in our earlier study (Sowell *et al.*, 2001). Finally, we created slope measures for the Sylvian fissure and superior temporal sulcus (i.e. length/height), and used Pearson correlation coefficients and *t*-tests to assess continuous age-effects and group differences in these measures.

Results

Sulcal Line Age-effects and Asymmetries

In Figure 4*A*, maps of sulcal line asymmetries for the average child, adolescent and adult groups are shown. A summary of the average asymmetries in the perisylvian sulci for the child, adolescent and young adult groups is also shown in Table 2. Note that the differences in millimeters between left and right hemisphere measures are based on orthogonal shift in the anterior–posterior or superior–inferior axes independently in Table 2. Displacement between the hemispheres shown in color in Figure 4 may seem greater because shifts in y and z axes are taken into account simultaneously as vectors. Note in Figure 4*A* the prominent and robust posterior temporal and postcentral gyral hemispheric asymmetries across all three age groups. The superior temporal sulcus extends 7–9 mm further back in the left hemisphere than the right in all subject groups (as shown in Table 2). The postcentral sulcus curves more anterior in the left in all three age groups, most prominently in the adolescents. The asymmetry in the Sylvian fissure, most notably in the posterior regions, is small in the children, somewhat pronounced in the adolescents and prominent in the young adults (on the order of 14–16 mm difference between the left and right hemispheres). The Sylvian fissure extends ~10 mm more posterior in the left hemisphere than in the right for the adolescents and adults, but only ~5 mm on average in the child group (as shown in Table 2).

Figure 4*B* is a sulcal line average map illustrating the differences in asymmetry between the children and young adults (expressed as a ratio of asymmetry in the children to asymmetry in the young adults). Note that the region with the most robust group difference is in the Sylvian fissure, where there is a 40–100% increase in asymmetry in the adults relative to the children, representing ~4–6 mm more asymmetry in the adults in more posterior regions (see Fig. 4*A*). Regions of reduced asymmetry in adults relative to children were observed in anterior inferior frontal gyrus, but these effects were much smaller (20% less asymmetry in adults than children). Figure 4*C* contains a statistical probability map of the child versus adult group difference in asymmetry (in the y–z axes). The statistical map is consistent with the ratio map of child versus adult asymmetry differences, showing that the regions with the most robust increases in asymmetry are statistically significantly different (at a sulcal line point threshold of $P = 0.05$) and localized primarily to the Sylvian fissure. Permutation tests were significant for the child versus adult asymmetry difference in the

Figure 6. Composite map where cortical gray matter density increase between childhood and young adulthood (expressed as a ratio of gray matter proportion in the child group to gray matter proportion in the adult group at each surface point) is shown on the average brain surface according to the color bar on the right. In these images, warmer colors are representative of regions where the proportion of gray matter is greater in the adults than in the children, with, at maximum, an ~25% increase in gray matter in the perisylvian region. The sulcal line probability map of age-related increase in asymmetry (see color bar on left) is laid over the cortical surface map of gray matter density increase. Note the spatial correspondence between regions of increased asymmetry and increased gray matter between childhood and young adulthood.

Figure 7. Probability maps of the correlation between sulcal asymmetry (as displacement in millimeters between the left and reflected right hemisphere shown in Fig. 4*A*) and gray matter density at each point along the Sylvian fissure in the left and right hemispheres in the child, adolescent and adult groups according the color bar on the right.

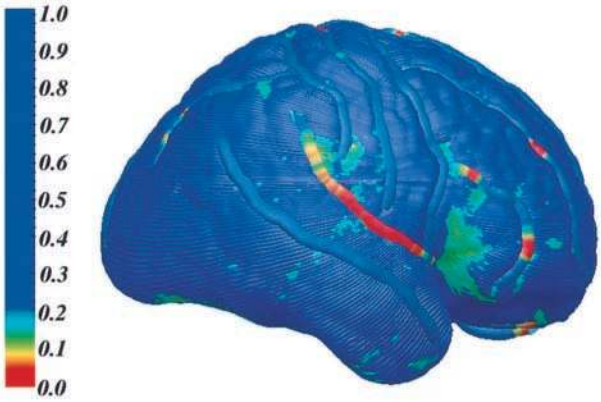

Sulcal Line Asymmetry
Age–effect P–map

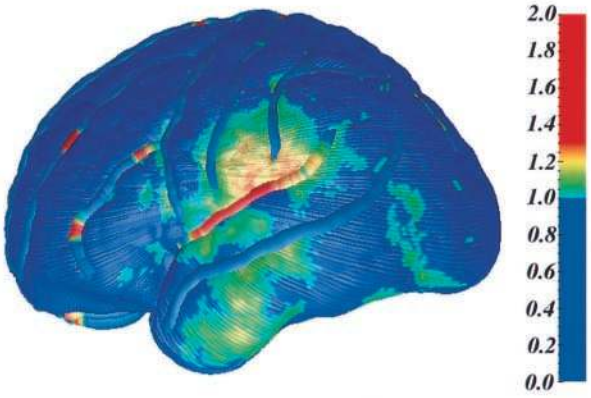

Surface Gray Matter
Increase Ratio Map

6

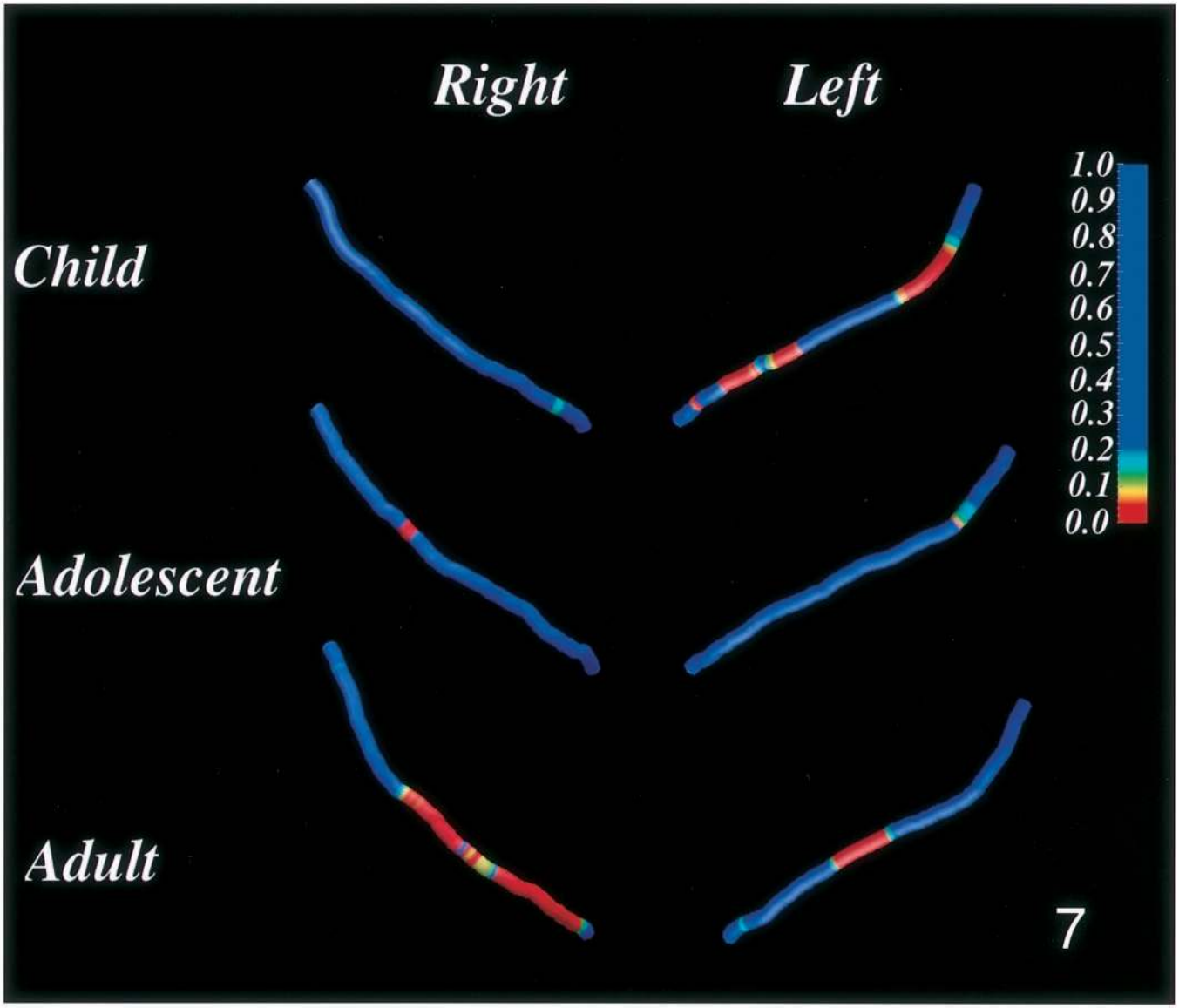

Sylvian fissure (P = 0.013), indicating that the extensive age effects in asymmetry in the Sylvian fissure do not occur by chance.

The slope of the Sylvian fissure was calculated as a ratio of the extent of the sulcal line in the anterior–posterior orthogonal axis over its extent in the superior–inferior orthogonal axis. Statistical tests show that the average slope in the right hemisphere becomes greater with age (r = 0.34, P < 0.05 with all 35 subjects) where the average angle of the right hemisphere Sylvian fissure relative to horizontal is 42° in the children and 47° in the adults. This is not true for the slope of the left hemisphere Sylvian fissure, which is the same in the children and the adults (38°). A Sylvian fissure slope asymmetry measure was at trend level significance for age effects. Frequency counts of the occurrence of right (R) greater versus left (L) greater slope asymmetries indicate that the children do not show strong asymmetries in either direction, with R > L slope occurring almost as frequently as L > R (~40% show R > L), in the adults; however, without exception, the slope in the right hemisphere is steeper than the left (r = 0.47, P = 0.044). Finally, in the right hemisphere, the Sylvian fissure and the superior temporal sulcus tend to be parallel in the children, but the slope of the Sylvian fissure becomes steeper than that of the superior temporal sulcus in adults (age effect of the ratio of Sylvian fissure slope over superior temporal sulcus slope, r = 0.36, P = 0.03 with all 35 subjects). This effect is not seen in the left hemisphere.

Brain Surface Characteristics, Sulcal Asymmetry and Gray Matter Proportion Relationships

Maps of intersubject cortical surface variability for the child group, adolescent group, and young adult group can be seen in Figure 5*A*. Essentially, this map illustrates the root mean square magnitude of displacement required to map each individual into each group's average space. Note that the pattern of variability across the cortex is similar in the three groups where greatest variability appears in the posterior temporal region and the postcentral gyrus. The variability is more prominent in the right hemisphere, where root mean square variability peaks at >12 mm in children, adolescents and in young adults. The least variability is observed in anterior, superior temporal and precentral sulci, and these findings are highly consistent with surface variability maps shown in other samples studied in our laboratory (Narr *et al*., 2001). Overall, the variability appears to be somewhat higher in the children than in the young adults. In Figure 5*B*, local cortical gray matter proportion maps for the average child brain, average adolescent brain and average young adult brain are presented. In all three groups, thinner cortex (lower regional gray matter proportion) is observed in primary motor and sensory cortices and in inferior parietal, lateral temporal and occipital lobes. Note that the regional pattern of gray matter proportion (within a 15 mm sphere at each brain surface point) also varies by age. For example, the gray matter proportion in the frontal cortex is on average >0.45 in the children and <0.45 in the young adults.

Figure 6 is a map of local gray matter proportion increase between childhood and young adulthood, expressed as a ratio of gray matter proportion at each brain surface point in the child group to the gray matter proportion at analogous surface points in the adult group. Note here the most prominent regions of gray matter proportion increases are in posterior–superior temporal and inferior parietal cortices bilaterally, greater in the left hemisphere. In this figure, we have overlaid the statistical map for differences between children and young adults in sulcal line asymmetry over the surface map of proportional increase in gray matter to highlight the spatial coincidence of localized age effects in gray matter density and age effects in Sylvian fissure asymmetry.

Finally, in Figure 7, we show the statistical maps of relationships between gray matter density and sulcal asymmetry at each point along the Sylvian fissure in each hemisphere in the child, adolescent and young adult groups. Note that the patterns vary by age, but it appears that Sylvian fissure asymmetries are more related to gray matter density in the adults than in the adolescents or the children. In other words, in adults, the greater the gray matter proportion along the Sylvian fissure, the greater the asymmetry in this region. The same does not appear to hold true in the children and adolescents, though we have not yet developed methods to assess age interactions in the relationship between gray matter density and sulcal asymmetry on a point-by-point basis.

Discussion

Findings of left longer than right and right more sloped than left Sylvian fissure asymmetries have been reported frequently in the adult *post mortem* (Geschwind and Galaburda, 1985) and *in vivo* imaging literatures (Thompson *et al*., 1998; Narr *et al*., 2001). Similar asymmetries have been observed perinatally (Witelson and Pallie, 1973), leading scientists to speculate that anatomic asymmetry is not entirely the result of environmental influences such as language learning and hand usage (Witelson, 1977). Results from this study imply that asymmetries in perisylvian cortices continue to develop between childhood and young adulthood. While the normal left longer than right Sylvian fissure asymmetry is present in children, adolescents and adults, it is much more pronounced in adulthood, on average twice the magnitude of the asymmetry observed in children. The asymmetry in the slope of the Sylvian fissure also changes with age such that the normal pattern of right more sloped than left occurred without exception in the young adults studied and significantly less frequently in the children.

The dynamic changes in asymmetry observed here seem to occur as a result of robust changes in the shape and location of the right hemisphere Sylvian fissure. The slopes of the Sylvian fissure and the superior temporal sulcus were roughly parallel in all three age groups in the left hemisphere, but in the right hemisphere the slope of the superior temporal sulcus remained constant in spite of the age-related upward slope of the Sylvian fissure. This is suggestive of an increase in the surface area of the posterior temporal lobes in the right hemisphere. It could also result from an anterior thrust of the right hemisphere parietal lobe, as suggested by Binder and colleagues (Binder *et al*., 1996). Developmental increases in the size and changing location of the parietal lobe could result in the increased Sylvian fissure slope with increasing age. Another research group reported that the frequency of duplication of Heschl's gyrus was approximately equal in the two hemispheres in the children, but more frequent in the right hemisphere in the adults (Leonard *et al*., 1998). This finding may be related to ours, given that in both studies the posterior Sylvian fissure asymmetry is more prominent in the adults and is attributable to right hemisphere differences. Leonard *et al*. (Leonard *et al*., 1998) suggest that their results are due to sampling differences between their children and adults rather than to maturation. Differences in methodology between the two studies make direct comparison of results difficult, but the converging evidence lends further credibility to the findings. Longitudinal studies over a broad age range (i.e. between childhood and young adulthood) will be required to definitively

determine the etiology of the phenomena observed by both groups.

Also revealed in this study are significant relationships between changes in perisylvian sulcal asymmetry and changes in local gray matter proportion within the underlying cortical tissue. Notably, the only regions in the brain which show age-related local cortical gray matter proportion increases spatially coincide with the only regions in the brain that show age-related changes in surface sulcal anatomy. Correlational analyses reveal that more mature patterns of gray matter proportion are related to more mature patterns of Sylvian fissure asymmetry, particularly in the young adult subjects. We observe these relationships despite the relatively large root mean square surface variability in the posterior temporal lobes, reflective of the amount of local deformation of the brain surface required to map each individual's brain into standard space. At first pass, gray matter density increases may seem incompatible with the developmental literature showing relative gray matter volume reductions between late childhood and young adulthood (Jernigan *et al.*, 1991; Sowell and Jernigan, 1998; Courchesne *et al.*, 2000). Additionally, we have shown spatially and temporally varying patterns of gray matter density reduction over large regions of dorsal and frontal cortices in these subjects in earlier reports, where voxel-based morphometric methods were used (Sowell *et al.*, 1999a,b). However, this is the first report where gray matter density has been measured at the cortical surface on a point-by-point basis utilizing manually defined cortical landmarks to match brain anatomy across subjects. These methods have resulted in greater spatial resolution for detecting regions of gray matter gain or loss in relatively close spatial proximity. Perhaps the relatively circumscribed region of gray matter gain was masked in the much larger region of the parietal and temporal lobes typically measured in volumetric studies. Further studies in different samples will be needed to confirm these findings.

In a recent longitudinal study, we observed prominent cerebral lobar growth in the lateral temporo-parietal region in children studied at various 2–4 year intervals between ~7 and 15 years of age (Thompson *et al.*, 2000a). This lobar growth was accompanied by a focus of extreme growth in the isthmus of the corpus callosum, the region that connects the temporo-parietal regions between the two hemispheres. Significant growth did not occur in any other callosal region, nor in any other area on the surface of the brain between 7 and 15 years in any of the five subjects studied serially. In another study of the same individuals studied in this report, we observed growth in the inferior, posterior temporal lobe occurring primarily between adolescence and adulthood (Sowell *et al.*, 2001). The maturation in the temporo-parietal cortices observed longitudinally and cross-sectionally may be consistent with the present findings of gray matter proportion increases between childhood and young adulthood specific to this region. Our observation of perisylvian sulcal asymmetry changes may also be related to growth in the callosal isthmus, given that correlations between these two structures have been observed in *post mortem* studies of adult males (Aboitiz *et al.*, 1992). Further studies will be needed to assess for age-related change in the relationship between perisylvian asymmetries and callosal morphometry.

The etiology of increased local gray matter proportion and sulcal asymmetry changes cannot be directly addressed with these data. Clearly, right hemisphere Sylvian fissure slope changes account more for the age effect in asymmetry than left hemisphere slope changes, while left hemisphere increases in local gray matter density are more prominent than right. None the less, Sylvian fissure asymmetry changes and changes in gray matter density are related as shown in the spatial (Fig. 6) and statistical (Fig. 7) analyses conducted here. It is possible that changes in Sylvian fissure morphology (or asymmetry) are indirect and secondary to changes in nearby cortical structures. For example, it is possible that shrinkage (i.e. synaptic pruning) of cortical tissue superior to the right hemisphere Sylvian fissure results in a passive rise in this structure as room is made within the superior part of the cranium. Conversely, perhaps increased slope with age in the left hemisphere Sylvian fissure is prevented by late growth (i.e. increased gray matter density) in the cortex superior to it. Notably, we assessed asymmetry only in the superior–inferior and anterior–posterior axes, ignoring age-related differences in the left–right direction. This was because we were most interested in asymmetries on the lateral surface of the brain in sulci oriented horizontally. Left–right shifts were thought to reflect increased sulcal depth (for sulci on the lateral brain surface), perhaps less interesting than shifts in sulcal location from an asymmetry perspective. It should be noted, however, that regional patterns of changes in sulcal depth could also be very interesting from a developmental perspective.

Maturational cellular events such as synaptic pruning (Huttenlocher, 1979), continued myelination (Yakovlev and Lecours, 1967) and perhaps even new neurons (Gould *et al.*, 1999) in perisylvian regions likely contribute to the dynamic changes in surface asymmetry and underlying gray matter proportion changes observed here between childhood and young adulthood. While the brain structural changes we observe are likely maturational in nature, we cannot rule out that individual differences in environmental influences (i.e. nutritional factors, environmental enrichment, educational changes) or other factors that vary with age (i.e. MRI image movement artefact more prominent in younger subjects) may also affect changes in the brain morphologic variables studied in this cross-sectional sample. Thus, it is important that these findings are replicated in separate samples and, ideally, studied longitudinally.

Notes

Support for this study was provided by grants NIMH K01MH01733 (to E.R.S.), P50 NS22343, R01 HD 23854, NIMH NRSA grant 5T32 MH16381, NSF DBI 9601356, the NCRR (P41 RR13642), NINDS (NS38753) and the pediatric supplement of the Human Brain Project, which is funded jointly by the NIMH and the NIDA (P20 MH/DA52176.

Address correspondence to Elizabeth R. Sowell, University of California, Los Angeles, Laboratory of Neuro Imaging, 710 Westwood Plaza, Room 4-238, Los Angeles, CA 90095-1769, USA. Email: esowell@loni.ucla.edu.

References

Aboitiz F, Scheibel AB, Zaidel E (1992) Morphometry of the Sylvian fissure and the corpus callosum, with emphasis on sex differences. Brain 115:1521–1541.

Benes FM, Turtle M, Khan Y, Farol P (1994) Myelination of a key relay zone in the hippocampal formation occurs in the human brain during childhood, adolescence, and adulthood. Arch Gen Psychiat 51:477–484.

Binder JR, Frost JA, Hammeke TA, Rao SM, Cox RW (1996) Function of the left planum temporale in auditory and linguistic processing. Brain 119:1239–1247.

Brodmann K (1909) Vergleichende Lokalisationlehre Der Grosshirnrinde in ihren' Prinzipien dargestellt auf Grund in Zellenbaues. Leipzig: J.A. Barth.

Caviness VS, Jr, Kennedy DN, Richelme C, Rademacher J, Filipek PA (1996) The human brain age 7–11 years: a volumetric analysis based on magnetic resonance images. Cereb Cortex 6:726–736.

Courchesne E, Chisum HJ, Townsend J, Cowles A, Covington J, Egaas B, Harwood M, Hinds S, Press GA (2000) Normal brain development and

aging: quantitative analysis at *in vivo* MR imaging in healthy volunteers. Radiology 216:672–682.

Evans AC, Kamber M, Collins DL, MacDonald D (1994) An MRI-based probabilistic atlas of neuroanatomy. In: Magnetic resonance scanning and epilepsy (Shorvon SD, ed.), pp. 263–274. New York: Plenum Press.

Galaburda AM, Sanides F, Geschwind N (1978) Human brain. Cytoarchitectonic left-right asymmetries in the temporal speech region. Arch Neurol 35:812–817.

Geschwind N, Galaburda AM (1985) Cerebral lateralization. Biological mechanisms, associations, and pathology: I. A hypothesis and a program for research. Arch Neurol 42:428–459.

Giedd JN, Blumenthal J, Jeffries NO, Castellanos FX, Liu H, Zijdenbos A, Paus T, Evans AC, Rapoport JL (1999) Brain development during childhood and adolescence: a longitudinal MRI study. Nat Neurosci 2:861–863.

Giedd JN, Snell JW, Lange N, Rajapakse JC, Casey BJ, Kozuch PL, Vaituzis AC, Vauss YC, Hamburger SD, Kaysen D, Rapoport JL (1996a) Quantitative magnetic resonance imaging of human brain development: ages 4–18. Cereb Cortex 6:551–560.

Giedd JN, Vaituzis AC, Hamburger SD, Lange N, Rajapakse JC, Kaysen D, Vauss YC, Rapoport JL (1996b) Quantitative MRI of the temporal lobe, amygdala, and hippocampus in normal human development: ages 4–18 years. J Comp Neurol 366:223–230.

Gould E, Reeves AJ, Graziano MS., Gross CG (1999) Neurogenesis in the neocortex of adult primates. Science 286:548–552.

Huttenlocher PR (1979) Synaptic density in human frontal cortex — developmental changes and effects of aging. Brain Res 163:195–205.

Huttenlocher PR, de Courten C (1987) The development of synapses in striate cortex of man. Hum Neurobiol 6:1–9.

Ide A, Rodriguez E, Zaidel E, Aboitiz F (1996) Bifurcation patterns in the human sylvian fissure: hemispheric and sex differences. Cereb Cortex 6:717–725.

Jernigan TL, Trauner DA, Hesselink JR, Tallal PA (1991) Maturation of human cerebrum observed *in vivo* during adolescence. Brain 114:2037–2049.

Kollokian V (1996) Performance analysis of automatic techniques for tissue classification in magnetic resonance images of human brain. Masters thesis, Concordia University.

LeMay M, Culebras A (1972) Human brain — morphologic differences in the hemispheres demonstrable by carotid arteriography. N Engl J Med 287:168–170.

Leonard CM, Puranik C, Kuldau JM, Lombardino LJ (1998) Normal variation in the frequency and location of human auditory cortex landmarks. Heschl's gyrus: where is it? Cereb Cortex 8:397–406.

MacDonald D, Avis D, Evans A (1994) Multiple surface identification and matching in magnetic resonance images. Proc Visualization Biomed Comput 2359:160–169.

Mazziotta JC, Toga AW, Evans A, Fox P, Lancaster J (1995) A probabilistic atlas of the human brain: theory and rationale for its development. The International Consortium for Brain Mapping (ICBM). Neuroimage 2:89–101.

Narr KL, Thompson PM, Sharma T, Moussai J, Zoumalan C, Rayman J, Toga AW (2001) Three-dimensional mapping of gyral shape and cortical surface asymmetries in schizophrenia: gender effects. Am J Psychiat 158:244–255.

Ono M, Kubik S, Abernathey CD (1990) Atlas of the cerebral sulci. Stuttgart: G. Thieme.

Paus T, Zijdenbos A, Worsley K, Collins DL, Blumenthal J, Giedd JN, Rapoport JL, Evans AC (1999) Structural maturation of neural pathways in children and adolescents: *in vivo* study. Science 283:1908–1911.

Pfefferbaum A, Mathalon DH, Sullivan EV, Rawles JM, Zipursky RB, Lim KO (1994) A quantitative magnetic resonance imaging study of changes in brain morphology from infancy to late adulthood. Arch Neurol 51:874–887.

Reiss AL, Abrams MT, Singer HS, Ross JL, Denckla MB (1996) Brain development, gender and IQ in children. A volumetric imaging study. Brain 119:1763–1774.

Sled JG, Zijdenbos AP, Evans AC (1998) A nonparametric method for automatic correction of intensity nonuniformity in MRI data. IEEE Trans Med Imaging 17:87–97.

Sowell ER, Jernigan TL (1998) Further MRI evidence of late brain maturation: limbic volume increases and changing asymmetries during childhood and adolescence. Dev Neuropsychol 14:599–617.

Sowell ER, Thompson PM, Holmes CJ, Batth R, Jernigan TL, Toga AW (1999a) Localizing age-related changes in brain structure between childhood and adolescence using statistical parametric mapping. Neuroimage 9:587–597.

Sowell ER, Thompson PM, Holmes CJ, Jernigan TL, Toga AW (1999b) *In vivo* evidence for post-adolescent brain maturation in frontal and striatal regions. Nature Neurosci 2:859–861.

Sowell ER, Thompson PM, Tessner KD, Toga AW (2001) Mapping continued brain growth and gray matter density reduction in dorsal frontal cortex: inverse relationships during postadolescent brain maturation. J Neurosci 21: 8819–8829.

Thompson PM, Toga AW (1996) A surface-based technique for warping three-dimensional images of the brain. IEEE Trans Med Imaging 15:402–417.

Thompson PM, Toga AW (1997) Detection, visualization and animation of abnormal anatomic structure with a deformable probabilistic brain atlas based on random vector field transformations. Med Image Anal 1:271–294.

Thompson PM, Toga AW (1998) Anatomically-driven strategies for high-dimensional brain image warping and pathology detection. In: Brain warping (Toga AW, ed.). San Diego, CA: Academic Press.

Thompson PM, MacDonald D, Mega MS, Holmes CJ, Evans AC, Toga AW (1997) Detection and mapping of abnormal brain structure with a probabilistic atlas of cortical surfaces. J Comput Assist Tomogr 21:567–581.

Thompson PM, Moussai J, Zohoori S, Goldkorn A, Khan AA, Mega MS, Small GW, Cummings JL, Toga AW (1998) Cortical variability and asymmetry in normal aging and Alzheimer's disease. Cereb Cortex 8:492–509.

Thompson PM, Giedd JN, Woods RP, MacDonald D, Evans AC, Toga AW (2000a) Growth patterns in the developing brain detected by using continuum mechanical tensor maps. Nature 404:190–193.

Thompson PM, Woods RP, Mega MS, Toga AW (2000b) Mathematical/computational challenges in creating deformable and probabilistic atlases of the human brain. Hum Brain Mapp 9:81–92.

Thompson PM, Mega MS, Woods RP, Zoumalan CI, Lindshield CJ, Blanton RE, Moussai J, Holmes CJ, Cummings JL, Toga AW (2001) Cortical change in Alzheimer's disease detected with a disease-specific population-based brain atlas. Cereb Cortex 11:1–16.

Von Economo CV (1929) The cytoarchitectonics of the human cerebral cortex. London: Oxford Medical.

Witelson SF (1977) Anatomic asymmetry in the temporal lobes: its documentation, phylogenesis, and relationship to functional asymmetry. Ann NY Acad Sci 299:328–354.

Witelson SF, Pallie W (1973) Left hemisphere specialization for language in the newborn. Neuroanatomical evidence of asymmetry. Brain 96:641–646.

Woods RP, Mazziotta JC, Cherry SR (1993) MRI–PET registration with automated algorithm. J Comput Assist Tomogr 17:536–546.

Wright IC, McGuire PK, Poline JB, Travere JM, Murray RM, Frith CD, Frackowiak RS, Friston KJ (1995) A voxel-based method for the statistical analysis of gray and white matter density applied to schizophrenia. Neuroimage 2:244–252.

Yakovlev PI, Lecours AR (1967) The myelogenetic cycles of regional maturation of the brain. In: Regional development of the brain in early life (Minkowski A, ed.), pp. 3–70. Oxford: Blackwell Scientific.